

Optimization of a $\text{CH}_3\text{NH}_3\text{SnI}_3$ based lead-free organic perovskite solar cell using SCAPS-1D simulator

Md. Sohel Rana, Md. Abdur Razzak

Department of Electrical and Electronic Engineering, Independent University, Bangladesh (IUB), Dhaka, Bangladesh

Article Info

Article history:

Received Aug 5, 2023

Revised Dec 6, 2023

Accepted Feb 12, 2024

Keywords:

$\text{CH}_3\text{NH}_3\text{SnI}_3$

Cu_2O

Lead-free perovskite

SCAPS-1D

TiO_2

ABSTRACT

In this study, a $\text{CH}_3\text{NH}_3\text{SnI}_3$ -based perovskite PV cell with the structure (FTO/ TiO_2 / $\text{CH}_3\text{NH}_3\text{SnI}_3$ / Cu_2O) was made and optimized by changing the layer thickness, defect density, and doping profile using the solar cell capacitance simulator (SCAPS) 1D simulator. To better understand how the device interface affects carrier dynamics, a synergic optimization of the device is done by altering the electron-transport layer (ETL) and hole-transport layer (HTL) materials. The light glows through the window layer of Sn_2O_3 : F, which serves as the transparent conducting oxide layer in our suggested cell construction and then travels over TiO_2 as an n-type ETL. Due to its unique features, the p-type perovskite ($\text{CH}_3\text{NH}_3\text{SnI}_3$) is chosen as the primary absorber layer. Lastly, Cu_2O is added as an HTL before the back contact because it has a higher hole conductivity and the proper offsets for spreading the valance and conduction bands. Additionally, Cu_2O -based devices outperform frequently utilized spiro-OMeTAD-based devices in terms of efficiency. According to the findings of these simulations, the optimized structure has a power conversion efficiency (PCE) of 41%, an open-circuit voltage of 1.32 V, a short-circuit current density of 34.31 mA/cm^2 and a fill factor (FF) of 90.5%. Additionally, the optimized structure has a short-circuit current density of 34.31 mA/cm^2 .

This is an open access article under the [CC BY-SA](https://creativecommons.org/licenses/by-sa/4.0/) license.



Corresponding Author:

Md. Abdur Razzak

Department of Electrical and Electronic Engineering, Independent University, Bangladesh (IUB)

Dhaka 1229, Bangladesh

Email: razzak@iub.edu.bd

1. INTRODUCTION

The modern world has already begun to experience an energy crisis due to its overreliance on fossil fuel energy, putting the future in grave peril. Researchers are looking towards sustainable, unrenowned, and environmentally benign alternative energy sources to address this looming threat. Solar energy is one of the most plentiful possibilities among all available energy sources. Solar cells use this energy and are considered clean and sustainable sources. Researchers are investigating several material compositions to create affordable and moderately efficient devices [1], [2]. Conventional silicon-based (C-Si) solar cells now dominate the photovoltaic market with a more than 90% share. This is due to silicon's ability to efficiently convert light into electricity power conversion efficiency (PCE) and its stability [3]. Theoretically, a C-Si-based solar cell exhibits a conversion efficiency of 26.7% under ideal room temperature conditions [4]. The production technique is costly relative to the performance improvement in real-world applications, and it has an indirect electronic band gap, making it a poor choice for long-wavelength sunlight.

All-inorganic perovskite has recently received much attention due to its superior thermal stability to organic cousins. The well-known formula for hybrid perovskite materials is ABX_3 , where X is a halogen monovalent anion (I, Br, or Cl⁻), and B is a metal divalent cation (such as Pb^{2+} , Sn^{2+} , or Ge^{2+}), a is an

organic monovalent cation (such as CH_3NH_3^+ or $\text{CH}_3(\text{NH}_2)^{2+}$). The inorganic C_sBX_3 compounds that are most frequently observed are CsPbI_3 , CsPbBr_3 , CsSnI_3 , and CsSnBr_3 . CsBX_3 is a promising material because of its higher absorption coefficients, high carrier mobilities, longer diffusion lengths, lower exciton-binding energy, excellent defect tolerance, and elastic energy gap. All of these characteristics contribute to a longer diffusion length [5]-[10]. Due to these characteristics, it is one of the materials that can be utilized for multi-junction or tandem solar cells. Additionally, due to the lead-free, non-toxic, all-inorganic perovskite PV technology's toxicity and moisture instability concerns, researchers have been moving away from lead-halide organic perovskite [11], [12]. Because of Sn's longer oxidation state, suitable absorption coefficient ($>10^5 \text{ cm}^{-1}$), ideal forbidden-gap (1.2-1.62 eV), and improved air stability, it is discovered that replacing lead (Pb) with Sn (tin) seems to be a good idea [13]-[17]. In particular, its derivative, $\text{CH}_3\text{NH}_3\text{SnI}_3$, acts as a favorable candidate for bulk-scale production. $\text{CH}_3\text{NH}_3\text{SnI}_3$ has also been researched as a hole-carrying element in dye-photosensitized PV cells, achieving good conversion efficiency. The most excellent efficiency of lead-free perovskite-based solar cells (PVSCs) has been attained for a thin-based structure at 13.24% [18]. Although all-inorganic PVSCs have grown significantly in recent years, they still trail behind their organic-inorganic counterparts, primarily because of considerable energy losses, flaws, and environmental instability. The absorber layer and its interface must be collectively optimized to improve the performance of all-inorganic PVSCs [19].

TiO_2 is the electron-transport layer (ETL) used most frequently and widely, even though it must be annealed at a high temperature. Ti possesses several desirable qualities, such as an affordable price, high electron mobility, low ecotoxicity, and stability. PCBM, on the other hand, is most frequently utilized in heterojunction cells (more precisely, for p-i-n structures). At the same time, ZnO and Sn provide good electron mobility, particularly for low-dimensional facilities. In this investigation, a $\text{CH}_3\text{NH}_3\text{SnI}_3$ -based perovskite PV cell with the following format ($\text{FTO}/\text{TiO}_2/\text{CH}_3\text{NH}_3\text{SnI}_3/\text{Cu}_2\text{O}$) was developed and then optimized with the use of the solar cell capacitance simulator (SCAPS) 1D simulator by altering the layer thickness, defect densities, and doping profiles. There have also been inquiries into how much of an effect temperature have at the point of operation. Illuminating the proposed cell structure is the TCO layer, composed of fluorine-doped tin oxide ($\text{Sn}_2\text{O:F}$). This layer also functions as the window layer. After that, an n-type electron transport layer made of Ti is applied, which begins to pull electrons from the absorber below it. Because of the distinctive qualities above, we have chosen the p-type perovskite ($\text{CH}_3\text{NH}_3\text{SnI}_3$) as the primary absorber layer. Finally, Cu_2O as a hole-transport layer (HTL) is added before the back contact due to its higher hole conductivity and appropriate offsets of valance and conduction band distribution, allowing for abrupt separation of the hole from the absorber. We chose Cu_2O for our device because it has the potential for more efficiency than the pricey, commonly used spiro-OMeTAD [20]. To examine the impact of the device interface on carrier dynamics and overall performance, a collective optimization of the device is also carried out by altering the materials for the ETL and HTL. Based on our simulations, the best structure has a PCE of 41%, an open-circuit voltage (V_{oc}) of 1.32 V, a short-circuit current (J_{sc}) density of $34.31 \text{ mA}/\text{cm}^2$, and a fill factor (FF) of 90%.

2. METHOD

The perovskite layer is placed between the HTL and ETL in a conventional planar device. The ETL and HTL must pick up the exactions made by light from the photo-excited perovskite absorber at the matching layer interfaces and send them to the outer circuit using the suitable bands. Our suggested planar solar cell has the TCO/ETL/absorber layer/HTL structure. TCO layer, fluorine doped tin oxide ($\text{Sn}_2\text{O:F}$), is the window layer in this cell construction. We used TiO_2 as an electron transport material (ETM) to extract electrons from the absorber since choosing the right ETL is crucial. The material for the absorber is perovskite ($\text{CH}_3\text{NH}_3\text{SnI}_3$), a p-type material with excellent electron/hole mobility and significant air stability. Finally, HTL, used before metal contact, was used to separate the hole from the absorber effectively. Moreover, as a hole transport material (HTM), we have used Cu_2O .

The SCAPS-1D simulation program/software was used to conduct the modeling and simulation in this work. 3D-dimensional simulator SCAPS (version 3307) uses position and continuity equations to model and simulate various solar designs. It allows for the input of seven semiconductor layers. The energy bands, concentrations and currents, J-V characteristics, ac characteristics (C and G) as functions of V and f, and spectral response (QE) may all be estimated using this simulator. Also calculable is the spectrum response. The simulation findings are more accurate than the experimental results, and this solar cell simulator has been frequently used to model CIGS and CdTe solar cells [21], [22]. Due to its user-friendly feature, simulations of perovskite solar cells using SCAPS software have recently begun to gain popularity. The structure of optimized solar cells is depicted in Figure 1, which shows that the thickness of each layer is optimized.

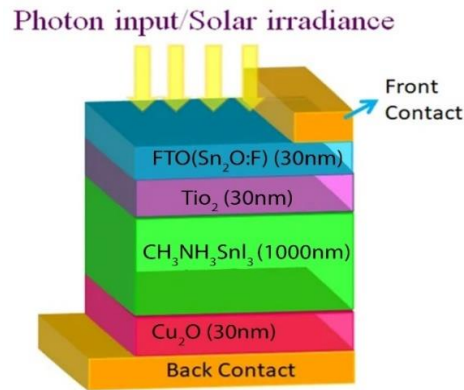


Figure 1. Schematic depiction of proposed PVSC cell at optimized thickness of all layers

This paper aimed to make the suggested structure work better to achieve the highest PCE at 1.5 AM solar insolation. This was done by adjusting the thicknesses, defect densities, series/shunt resistances, temperatures, and doping profiles of the window, absorber, TCO, and transport layers. This was done to achieve the best possible PCE. Our system's best HTL is Cu_2O , and the best ETL is TiO_2 . This was found through a process called synergistic optimization. We found that the best consistency for our proposed optimized cell is 1 μm of p-type perovskite as the absorber and 30 nm of Cu_2O as the high-temperature layer. Together, these two layers make up the optimal thickness of the cell. Light first enters the cell through the TCO, a window layer. It then travels across the electron transport layer (n-type TiO_2), also serving as a buffer layer. After that, light enters the absorber layer and eventually reaches the whole transport material.

The properties of all of the main design parameters that are utilized to define how the photo-generated carriers travel and how well the optimized structure functions are displayed in Table 1. This data was compiled with the help of trustworthy information sources. The electron affinity (χ) affects how the bands are offset at the device interfaces. The relative permittivity (ϵ_r) is shown here. N_C and N_V are the standard effective densities of states for the conduction band and the valence band, respectively. Although N_D and N_A stand for the donor and acceptor densities, conventional n and p refer to the mobility of electrons and holes, respectively. N_D and N_A are abbreviations. It is essential to remember that the thermal velocity of the electrons and holes is always held at 1×10^7 cm. The defect charge density throughout the entire area is consistent, and the defects have no discernible pattern. The gaussian energy distribution of the defect level is set to 1, as is the capture cross section for both electrons and holes. According to the literature [23]-[30] N_t , the total defect density, is chosen.

Table 1. The parameters table of different layer of proposed solar cell

Parameter	FTO	TiO_2 (n)	$\text{CH}_3\text{NH}_3\text{SnI}_3$ (p)	Cu_2O (p)
Thickness (μm)	0.03	0.03	Varied	0.03
E_g (eV)	3.5	3.260	1.3	2.1
χ (eV)	4.00	4.200	4.1	3.2
ϵ_r	9.00	10.000	6.5	6.6
N_C (cm^{-3})	2.200E+18	2.20E+18	1.000E+18	2.500E+20
N_V (cm^{-3})	1.800E+18	1.8E+18	1.000E+19	2.500E+20
μ_n (cm^2/Vs)	2.000E+1	2.000E+1	1.6	80
μ_p (cm^2/Vs)	1.00E+1	1.000E+1	1.6	80
N_D (cm^{-3})	1.0E+19	1.00E+17	0	0
N_A (cm^{-3})	0	0	1.000E+22	3.600E+18

3. RESULTS AND DISCUSSION

In this part, the research findings are discussed while also providing an in-depth analysis. Results can be shown in tables, graphs, and figures in the following sections.

3.1. Variation of doping concentration in the absorber layers

This subsection summarizes the changes in performance parameters brought on by variations in doping densities in the absorbing layers. Doping is a crucial factor that determines the performance spectrum

of any solar cell design. The material properties might benefit or negatively affect the device as a whole, depending on the kind [31]. It is essential to optimize the doping concentration in the absorber layers to increase efficiency. Studies have shown that unfavorable or excessive doping attention might impact the total carrier density and produce unreliable flaws, restricting the carriers' transit. As a result, the device's stability is altered, and the overall PCE is decreased. We changed the concentration from $1 \times 10^{10} \text{ cm}^{-3}$ to $1 \times 10^{22} \text{ cm}^{-3}$ to observe the effects of both high and low doping densities to have a clear view of the effects of doping on cell performance. Figure 2 shows that as the acceptor doping density goes up, the V_{oc} , the FF (%), and the efficiency (%) all go up by a lot, significantly above $1 \times 10^{19} \text{ cm}^{-3}$ acceptor doping density. As the doping density goes up, so do the charges. This makes the V_{oc} go up by a lot. At $1 \times 10^{22} \text{ cm}^{-3}$ acceptor doping density, the efficiency increases by 39%, and the FF increases by 90%.

3.2. Effect of defect density variation of the perovskite layer

As the generation, recombination, and transportation processes all take place inside the absorber layer, the quality of the absorber, such as the number of defects, is one of the critical factors affecting the performance of solar cells [32]. These layers were the starting point for most photovoltaic processes, including forming electron-hole pairs, recombination, and carrier movement. It is now well acknowledged that these activities are fundamental components of the absorber layer that makes up the structure of a solar cell. The overall quality, molecular chemistry, and fabrication technique of an absorber layer have all been demonstrated to impact a device's performance significantly. This is accomplished by reducing the lifespan of the device and the diffusion length for carriers [33]-[35]. Therefore, to optimize the device's overall performance, it is necessary to adjust the defect density to an optimum value. This is because the defect density can play a significant role in effectively influencing the performance characteristics of a structure.

Due to the simplicity of the calculation process, the defect concentrations in the absorber layer may frequently be ignored during the simulation step. However, fabrication mistakes can be made that alter performance variables. The absorber material's fault density was altered during the simulation of this solar cell from $1 \times 10^{10} \text{ cm}^{-3}$ to $1 \times 10^{22} \text{ cm}^{-3}$ at the cell's ideal thickness. As seen in Figure 3, the characteristic parameters all fell gradually as the defect density increased to $1 \times 10^{15} \text{ cm}^{-3}$. Still, they all abruptly decreased after that point and reached their lowest value at $1 \times 10^{22} \text{ cm}^{-3}$. The most insufficient numbers are 0.26% for PCE, 87% for FF, 0.98 for V_{oc} , and 0.30 for J_{sc} . After $1 \times 10^{15} \text{ cm}^{-3}$, the recombination current significantly increased, causing a sharp decline in the cell's J_{sc} . Therefore, this cell structure may perform rationally with a crystal defect, but not more than $1 \times 10^{15} \text{ cm}^{-3}$.

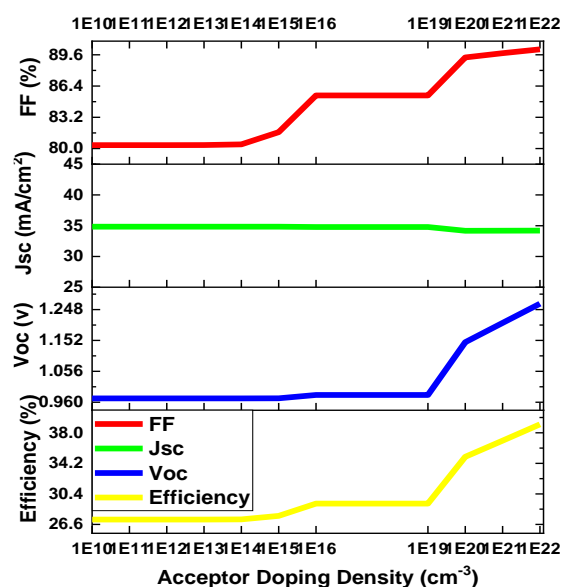


Figure 2. The impact of variation of acceptor doping density on J_{sc} , V_{oc} , FF, and efficiency

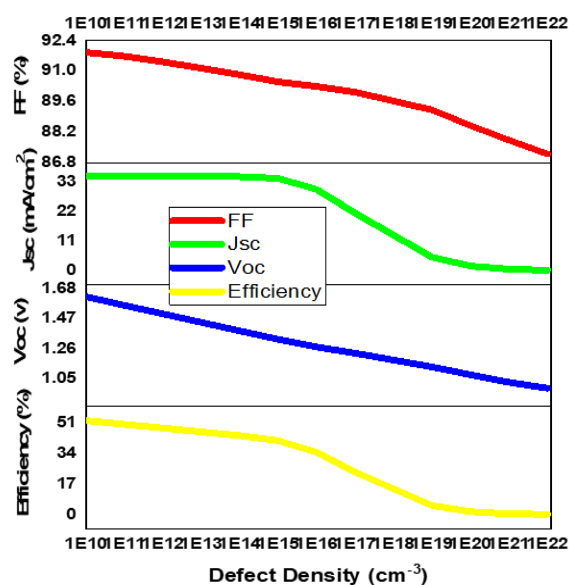


Figure 3. Effects of defect density of absorber layer on whole cell performance

3.3. Effect of thickness variation of absorber layer on device performance

The absorber layer thickness is the primary factor affecting a solar cell's fundamental parameters. These properties include J_{sc} , V_{oc} , FF, and PCE. With increased absorber layer thickness comes an increased

capacity to absorb photons with longer wavelengths, which is necessary to produce photo-generated excitons. The J_{sc} rises due to the surge of charge carriers, improving efficiency [36], [37]. Maximum efficiency is possible at the ideal absorber height because it efficiently absorbs and separates the photo-generated carrier [38]. Conversely, experimentation has demonstrated that a thicker absorber has trouble extracting charge carriers due to a decreasing electric field, which lowers cell PCE [39]. Due to a rise in the likelihood of recombination and series resistance in the absorber layer, the V_{oc} , and FF decrease with thickness. In this case, the batch calculation mode in SCAPS 1D was used to figure out how well the proposed cell would work while at the same time changing the thickness of the absorber layer, as shown in Figure 4. By maintaining the acceptor doping concentration constant at the optimized level of $1 \times 10^{22} \text{ cm}^{-3}$ (optimization of the doping profile is discussed in subsection, 3.1, we aimed to comprehend the performance and identify the ideal thickness of it). Figure 4 demonstrates that this solar cell begins to operate at a thickness of 0.005 μm , the lowest thickness needed to capture photons and produce electron-hole pairs. Figure 5 shows that with increasing the temperature, the V_{oc} decreased linearly from 1.2 V to 1.1 V. The improvement in J_{sc} and efficiency is significant when absorber thickness increases from 0.1 μm to 1 μm . When the thickness of the absorber was increased from 0.1 μm to 1 μm , a substantial improvement in J_{sc} and efficiency was observed. The J_{sc} goes from 19 mA/cm^2 to 34 mA/cm^2 , whereas the PCE goes from 23% to 41%.

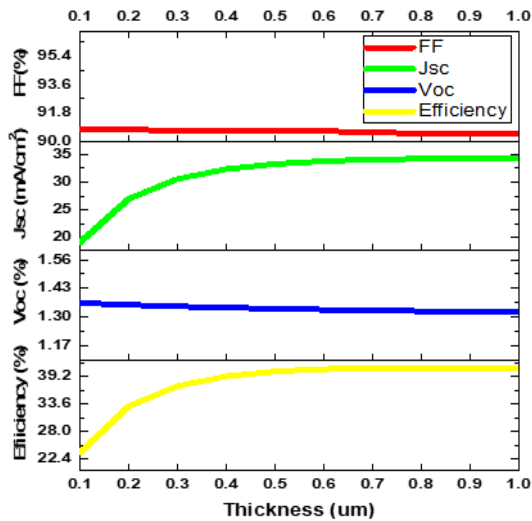


Figure 4. The impact of variation of absorber layer thicknesses on J_{sc} , V_{oc} , FF, and efficiency

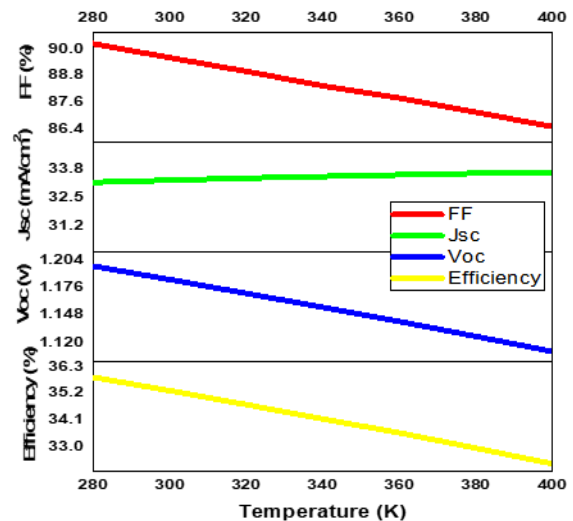


Figure 5. Effects of temperature on whole cell performances

3.4. Variation of operating temperature for the proposed cell

The operating temperature of a PSC is typically one of the most significant factors that can determine whether or not it can work as planned. Any distortion between the layers, whether due to the materials' purity or an error that happens unintentionally during the fabrication process, can cause an increase in temperature. Nevertheless, any of these factors, including the potential for an increase in temperature within the cell's structure, could significantly impact the stability of the apparatus while it is in use. This drop in V_{oc} , reduced efficiency from 36% to 32.3%, and the FF decreased from 90% to 86%. However, a minor raise in J_{sc} is seen here because of released free charge carriers owing to the loosening of atomic bonds with elevated temperature.

3.5. Variation of series and shunt resistance of our proposed structure

A solar cell device's performance is also greatly influenced by series resistance, notably the FF and J_{sc} density. The value of the FF also begins to decrease, which is a consequence of the reduction in the short-circuit current that occurs when the series resistance is increased. On the other hand, this results in a reduction in the overall efficiency of the solar cell. The shunt resistance (R_{sh}) of a solar cell can result in yet another considerable loss of power. The shunt resistance is often produced due to manufacturing faults during fabrication rather than a flawed solar design. Because of this, the parameter is a crucial aspect to consider for the purpose of making a realistic estimate of the solar system's performance in real life. Lower levels of shunt resistance can provide the carriers with an alternative channel down which they can tunnel. This can result in

a considerable loss of power, affecting performance metrics. Because lower carriers would initially be generated while concurrently recombining internally, the repercussions can become significantly more severe in settings with less light.

Here we examined series resistance from 100 mOhm.cm² to 1000 mOhm.cm², and shunt resistance varied from 100 Ohm.cm² to 1000 Ohm.cm² to understand the impact of parasitic resistance. As shown in Figure 6, the bulk resistance of the absorber material increased, as did the resistance along the carrier transportation path. As a result, the short-circuit current density decreased as the series resistance grew, resulting in a decline in the system's efficiency. V_{oc} , then produces with increasing R_{sh} to 0.947 V, shown in Figure 7. The mechanism for this occurs because conductive routes through p-n junctions or on cell borders become more resistant when R_{sh} increases, which reduces the number of leakage carriers. Beyond R_{sh} of 1000 Ohm.cm², this charge leakage becomes negligible.

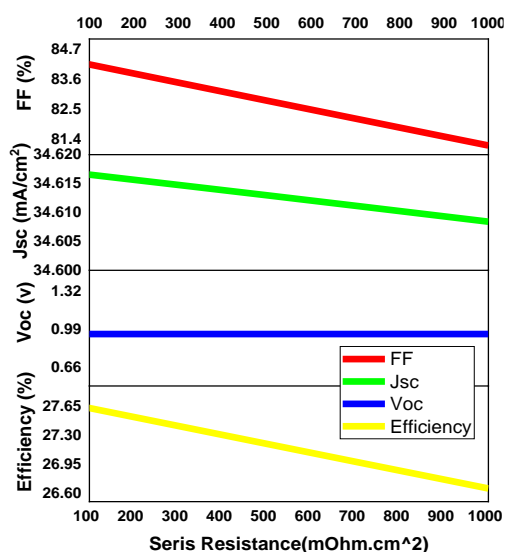


Figure 6. The effects of variation of series resistance on J_{sc} , V_{oc} , FF, and efficiency

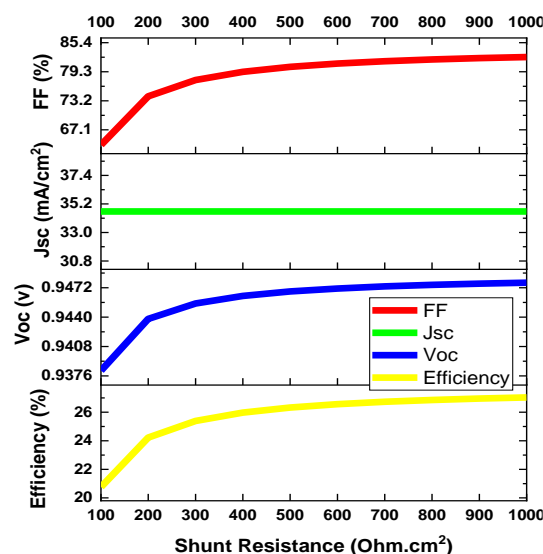


Figure 7. Impacts of shunt resistance on whole cell performance

3.6. The optimized performance investigation

In this study, we simulate the performance features of our proposed solar cell architecture by adjusting various parameters one at a time while maintaining the other factors constant. This procedure is reflected in the study. After that, the performance criteria, which include J_{sc} , V_{oc} , PEC, and FF, determine the highest possible quantity for that category. The study gives an overview of how to improve different types of absorbers, such as their thickness, the effect of doping, the number of flaws, the results of series shunt resistance, and the change in operating temperature. At the end of the process, we were able to finalize a solar cell structure as FTO/TiO₂/CH₃NH₃SnI₃/Cu₂O. For the final simulation, we got a J_{sc} value of 34.31 mA/cm², a V_{oc} value of 1.32 V, a PCE value of 41%, and an FF value of 90%. You can see these numbers in Figure 8, which shows the J-V curve of our finished device.

Figure 9 depicts the quantum efficiency (QE) curve and the relationship between photon energy and wavelength. The graph reveals that the convection efficiency of the device increases with an increase in the wavelength of the light, reaching its highest point when the wavelength of the light is increased. Light with a wavelength of more than 850 nm contains nearly enough power to absorb a material bandgap; nevertheless, the energy of a photon gradually decreases as the wavelength of light increases. This leads to an exponential decline in the efficiency of QE. Because the energy of this photon is lower than the bandgap of absorbers, light with a wavelength of more than 960 nanometers cannot generate electrons. This results in a significant increase in the recombination current of the solar cell that has been proposed, as can be seen in Figure 8. Therefore, the absorbance range for this device is 300–960 nm⁻³, which is a statement we can confidently make. The planned work is also compared to works published in the past, as shown in Table 2. Compared to the designs that came before it, the performance of the design that has been proposed is significantly superior.

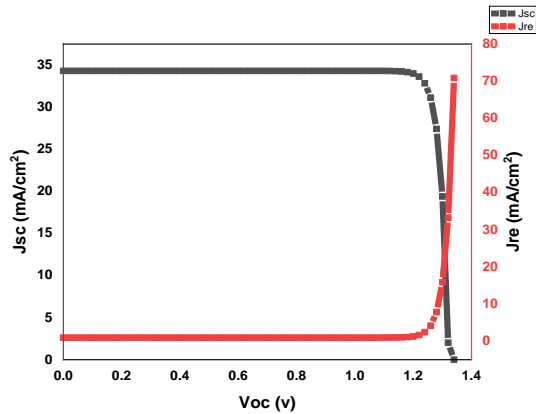


Figure 8. J-V graph of optimized solar cell

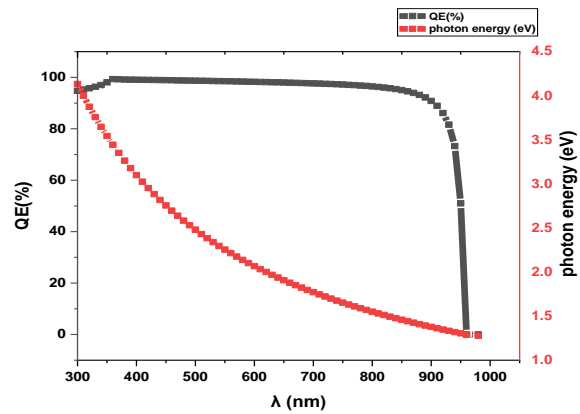


Figure 9. QE of proposed solar cell

Table 2. Comparison of the proposed work with various previously published works

Ref.	Model	Efficiency (%)
[40]	NiO/CH ₃ NH ₃ SnI ₃ /PCBM	22.95
[41]	FTO/TiO ₂ /CH ₃ NH ₃ SnI ₃ /Ni	26.33
[42]	FTO/TiO ₂ /CH ₃ NH ₃ SnI ₃ /Cu ₂ O	28.39
[43]	TCO/TiO ₂ /CH ₃ NH ₃ SnI ₃ /Cu	32.13
This work	FTO/TiO ₂ /CH ₃ NH ₃ SnI ₃ /Cu ₂ O	41

4. CONCLUSION




This work has constructed and simulated a skinny (1 m) organic Cs₂SnI₆-based perovskite PV cell with an FTO/TiO₂/CH₃NH₃SnI₃/Cu₂O structure. This was accomplished by optimizing the layer thickness at 1.09 μm, defect densities at 1×10¹⁵ cm⁻³, doping densities at 1×10²² cm⁻³, 1000 Ohm/cm² shunt resistance, and 100 mOhm. When the p-type HTL layer is Cu₂O, and the suitable n-type ETL is TiO₂, isolating the photo-generated carrier well, the PCE can be as high as 41%. The simulation results indicate that they significantly achieved such high-PCE. The results of our simulations reveal that the proposed cell structure generated a V_{oc} of 1.32 volts, a short-circuit current density of 34.31 mA/cm² and an FF of 90% at an operating temperature of 300 K under 1.5 ampere-hours of solar irradiation.

REFERENCES




- [1] S. Bhattacharya and S. John, "Beyond 30% Conversion Efficiency in Silicon Solar Cells: A Numerical Demonstration," *Sci. Rep.*, vol. 9, no. 1, p. 12482, Aug. 2019, doi: 10.1038/s41598-019-48981-w.
- [2] M. Grätzel, "The light and shade of perovskite solar cells," *Nat. Mater.*, vol. 13, no. 9, pp. 838–842, Sep. 2014, doi: 10.1038/nmat4065.
- [3] R. Kour *et al.*, "Potential Substitutes for Replacement of Lead in Perovskite Solar Cells: A Review," *Glob. Challenges*, vol. 3, no. 11, p. 1900050, Nov. 2019, doi: 10.1002/gch2.201900050.
- [4] W. Shockley and H. J. Queisser, "Detailed Balance Limit of Efficiency of p-n Junction Solar Cells," *J. Appl. Phys.*, vol. 32, no. 3, pp. 510–519, Mar. 1961, doi: 10.1063/1.1736034.
- [5] M. Konstantakou and T. Stergiopoulos, "A critical review on tin halide perovskite solar cells," *J. Mater. Chem. A*, vol. 5, no. 23, pp. 11518–11549, 2017, doi: 10.1039/C7TA00929A.
- [6] J. Zhang, G. Hodes, Z. Jin, and S. (Frank) Liu, "All-Inorganic CsPbX₃ Perovskite Solar Cells: Progress and Prospects," *Angew. Chemie Int. Ed.*, vol. 58, no. 44, pp. 15596–15618, Oct. 2019, doi: 10.1002/anie.201901081.
- [7] S. De Wolf *et al.*, "Organometallic Halide Perovskites: Sharp Optical Absorption Edge and Its Relation to Photovoltaic Performance," *J. Phys. Chem. Lett.*, vol. 5, no. 6, pp. 1035–1039, Mar. 2014, doi: 10.1021/jz500279b.
- [8] P. Todorović *et al.*, "Spectrally Tunable and Set al Electroluminescence Enabled by Rubidium Doping of CsPbBr₃ Nanocrystals," *Adv. Opt. Mater.*, vol. 7, no. 24, p. 1901440, Dec. 2019, doi: 10.1002/adom.201901440.
- [9] R. L. Milot *et al.*, "Charge-Carrier Dynamics in 2D Hybrid Metal–Halide Perovskites," *Nano Lett.*, vol. 16, no. 11, pp. 7001–7007, Nov. 2016, doi: 10.1021/acs.nanolett.6b03114.
- [10] Q. A. Akkerman, G. Rainò, M. V. Kovalenko, and L. Manna, "Genesis, challenges and opportunities for colloidal lead halide perovskite nanocrystals," *Nat. Mater.*, vol. 17, no. 5, pp. 394–405, May 2018, doi: 10.1038/s41563-018-0018-4.
- [11] B. Parida, S. Yoon, S. M. Jeong, J. S. Cho, J.-K. Kim, and D.-W. Kang, "Recent progress on cesium lead/tin halide-based inorganic perovskites for stable and efficient solar cells: A review," *Sol. Energy Mater. Sol. Cells*, vol. 204, p. 110212, Jan. 2020, doi: 10.1016/j.solmat.2019.110212.
- [12] Y. C. Choi and K.-W. Jung, "Recent Progress in Fabrication of Antimony/Bismuth Chalcogenides for Lead-Free Solar Cell Applications," *Nanomaterials*, vol. 10, no. 11, p. 2284, Nov. 2020, doi: 10.3390/nano10112284.
- [13] T. C. Jellicoe *et al.*, "Synthesis and Optical Properties of Lead-Free Cesium Tin Halide Perovskite Nanocrystals," *J. Am. Chem. Soc.*, vol. 138, no. 9, pp. 2941–2944, Mar. 2016, doi: 10.1021/jacs.5b13470.

- [14] B. Lee *et al.*, "Air-Stable Molecular Semiconducting Iodosalts for Solar Cell Applications: Cs₂SnI₆ as a Hole Conductor," *J. Am. Chem. Soc.*, vol. 136, no. 43, pp. 15379–15385, Oct. 2014, doi: 10.1021/ja508464w.
- [15] S. Ullah *et al.*, "Fabrication and characterization of lead-free Cs₂SnI₆ perovskite films for photovoltaic applications," *Int. J. Energy Res.*, vol. 45, no. 2, pp. 1720–1728, Feb. 2021, doi: 10.1002/er.5838.
- [16] S. Ghosh, S. Paul, and S. K. De, "Control Synthesis of Air-Stable Morphology Tunable Pb-Free Cs₂SnI₆ Perovskite Nanoparticles and Their Photodetection Properties," *Part. Part. Syst. Charact.*, vol. 35, no. 9, p. 1800199, Sep. 2018, doi: 10.1002/ppsc.201800199.
- [17] X. Qiu *et al.*, "From unstable CsSnI₃ to air-stable Cs₂SnI₆: A lead-free perovskite solar cell light absorber with bandgap of 1.48 eV and high absorption coefficient," *Sol. Energy Mater. Sol. Cells*, vol. 159, pp. 227–234, Jan. 2017, doi: 10.1016/j.solmat.2016.09.022.
- [18] K. Nishimura *et al.*, "Lead-free tin-halide perovskite solar cells with 13% efficiency," *Nano Energy*, vol. 74, p. 104858, Aug. 2020, doi: 10.1016/j.nanoen.2020.104858.
- [19] J. Tian, Q. Xue, Q. Yao, N. Li, C. J. Brabec, and H. Yip, "Inorganic Halide Perovskite Solar Cells: Progress and Challenges," *Adv. Energy Mater.*, vol. 10, no. 23, p. 2000183, Jun. 2020, doi: 10.1002/aenm.202000183.
- [20] M. Shasti and A. Mortezaali, "Numerical Study of Cu₂O, SrCu₂O₂, and CuAlO₂ as Hole-Transport Materials for Application in Perovskite Solar Cells," *Phys. status solidi*, vol. 216, no. 18, p. 1900337, Sep. 2019, doi: 10.1002/pssa.201900337.
- [21] K. Decock, P. Zabierowski, and M. Burgelman, "Modeling metastabilities in chalcopyrite-based thin film solar cells," *J. Appl. Phys.*, vol. 111, no. 4, p. 043703, Feb. 2012, doi: 10.1063/1.3686651.
- [22] A. Niemegeers and M. Burgelman, "Numerical modelling of AC-characteristics of CdTe and CIS solar cells," in *Conference Record of the Twenty Fifth IEEE Photovoltaic Specialists Conference - 1996*, 1996, pp. 901–904, doi: 10.1109/PVSC.1996.564274.
- [23] D. Liu, J. Yang, and T. L. Kelly, "Compact Layer Free Perovskite Solar Cells with 13.5% Efficiency," *J. Am. Chem. Soc.*, vol. 136, no. 49, pp. 17116–17122, Dec. 2014, doi: 10.1021/ja508758k.
- [24] W. Ke *et al.*, "Efficient hole-blocking layer-free planar halide perovskite thin-film solar cells," *Nat. Commun.*, vol. 6, no. 1, p. 6700, Mar. 2015, doi: 10.1038/ncomms7700.
- [25] L. Huang *et al.*, "Efficient planar perovskite solar cells without a high temperature processed titanium dioxide electron transport layer," *Sol. Energy Mater. Sol. Cells*, vol. 149, pp. 1–8, May 2016, doi: 10.1016/j.solmat.2015.12.033.
- [26] M. Hirasawa, T. Ishihara, T. Goto, K. Uchida, and N. Miura, "Magnetoabsorption of the lowest exciton in perovskite-type compound (CH₃NH₃)PbI₃," *Phys. B Condens. Matter*, vol. 201, pp. 427–430, Jul. 1994, doi: 10.1016/0921-4526(94)91130-4.
- [27] M. M. Tavakoli *et al.*, "Highly Efficient Flexible Perovskite Solar Cells with Antireflection and Self-Cleaning Nanostructures," *ACS Nano*, vol. 9, no. 10, pp. 10287–10295, Oct. 2015, doi: 10.1021/acsnano.5b04284.
- [28] N. Torabi, A. Rahnamanic, H. Amrollahi, F. Mirjalili, M. A. Sadeghzade, and A. Behjat, "Performance enhancement of perovskite solar cell by controlling deposition temperature of copper phthalocyanine as a dopant-free hole transporting layer," *Org. Electron.*, vol. 48, pp. 211–216, Sep. 2017, doi: 10.1016/j.orgel.2017.06.007.
- [29] T. M. Razykov, A. X. Shukurov, O. K. Atabayev, K. M. Kuchkarov, B. Ergashev, and A. A. Mavlonov, "Growth and characterization of Sb₂Se₃ thin films for solar cells," *Sol. Energy*, vol. 173, pp. 225–228, Oct. 2018, doi: 10.1016/j.solener.2018.07.082.
- [30] F. Anwar, R. Mahbub, S. S. Satter, and S. M. Ullah, "Effect of Different HTM Layers and Electrical Parameters on ZnO Nanorod-Based Lead-Free Perovskite Solar Cell for High-Efficiency Performance," *Int. J. Photoenergy*, vol. 2017, pp. 1–9, 2017, doi: 10.1155/2017/9846310.
- [31] T. H. Schloemer, J. A. Christians, J. M. Luther, and A. Sellinger, "Doping strategies for small molecule organic hole-transport materials: impacts on perovskite solar cell performance and stability," *Chem. Sci.*, vol. 10, no. 7, pp. 1904–1935, 2019, doi: 10.1039/C8SC05284K.
- [32] K. Yang, B. Li, and G. Zeng, "Structural, morphological, compositional, optical and electrical properties of Sb₂Se₃ thin films deposited by pulsed laser deposition," *Superlattices Microstruct.*, vol. 145, p. 106618, Sep. 2020, doi: 10.1016/j.spmi.2020.106618.
- [33] J. M. Ball, M. M. Lee, A. Hey, and H. J. Snaith, "Low-temperature processed meso-superstructured to thin-film perovskite solar cells," *Energy Environ. Sci.*, vol. 6, no. 6, p. 1739, 2013, doi: 10.1039/c3ee40810h.
- [34] J. Barbé *et al.*, "Amorphous Tin Oxide as a Low-Temperature-Processed Electron-Transport Layer for Organic and Hybrid Perovskite Solar Cells," *ACS Appl. Mater. Interfaces*, vol. 9, no. 13, pp. 11828–11836, Apr. 2017, doi: 10.1021/acsmi.6b13675.
- [35] H. Kim, K.-G. Lim, and T.-W. Lee, "Planar heterojunction organometal halide perovskite solar cells: roles of interfacial layers," *Energy Environ. Sci.*, vol. 9, no. 1, pp. 12–30, 2016, doi: 10.1039/C5EE02194D.
- [36] Y. Liu *et al.*, "Solution-processed small-molecule solar cells: breaking the 10% power conversion efficiency," *Sci. Rep.*, vol. 3, no. 1, p. 3356, Nov. 2013, doi: 10.1038/srep03356.
- [37] H. Chen *et al.*, "Enhanced Performance of Planar Perovskite Solar Cells Using Low-Temperature Solution-Processed Al-Doped SnO₂ as Electron Transport Layers," *Nanoscale Res. Lett.*, vol. 12, no. 1, p. 238, Dec. 2017, doi: 10.1186/s11671-017-1992-1.
- [38] S. M. U. F. Anwar, R. Mahbub, and S. S. Satter, "Effect of Doping on the Structural, Morphological, and Optical Properties of ZnO Thin Films Prepared by Spray Pyrolysis," *Int. J. Photoenergy*, 2017.
- [39] J.-P. Correa-Baena *et al.*, "Promises and challenges of perovskite solar cells," *Science (80-.)*, vol. 358, no. 6364, pp. 739–744, Nov. 2017, doi: 10.1126/science.aam6323.
- [40] M. S. Shamna, K. S. Nithya, and K. S. Sudheer, "Simulation and optimization of CH₃NH₃SnI₃ based inverted perovskite solar cell with NiO as Hole transport material," *Mater. Today Proc.*, vol. 33, pp. 1246–1251, 2020, doi: 10.1016/j.matpr.2020.03.488.
- [41] A. Sunny, S. Rahman, M. M. Khatun, and S. R. Al Ahmed, "Numerical study of high performance HTL-free CH₃NH₃SnI₃-based perovskite solar cell by SCAPS-1D," *AIP Adv.*, vol. 11, no. 6, p. 065102, Jun. 2021, doi: 10.1063/5.0049646.
- [42] P. K. Patel, "Device simulation of highly efficient eco-friendly CH₃NH₃SnI₃ perovskite solar cell," *Sci. Rep.*, vol. 11, no. 1, p. 3082, Feb. 2021, doi: 10.1038/s41598-021-82817-w.
- [43] S. Imani, S. M. Seyed-Talebi, J. Beheshtian, and E. W. G. Diau, "Simulation and characterization of CH₃NH₃SnI₃-based perovskite solar cells with different Cu-based hole transporting layers," *Appl. Phys. A*, vol. 129, no. 2, p. 143, Feb. 2023, doi: 10.1007/s00339-023-06428-0.

BIOGRAPHIES OF AUTHORS

Md. Sohel Rana    graduated from Prime University in Bangladesh in 2015 with a Bachelor of Science in Electrical and Electronic Engineering. He was awarded this degree in 2015. In 2018, he got a Master of Science in Telecommunication Engineering from the University of Information Technology and Sciences (UITS), Bangladesh. He completed M.Sc. Engineering (M.Sc. in Engineering in Information Systems Security) from Bangladesh University of Professionals (BUP), Bangladesh in 2022. He is currently studying for a M.Sc. program at Independent University, Bangladesh (IUB), in the Department of Electrical and Electronic Engineering. His research interests include microstrip patch antennas, wireless communication, image processing, renewable energy, solar cell, biomedical engineering, control system, and power electronics. He authored and co-authored in 40 papers regarding to his research works. At present, he is working as a Lecturer and Head (In-Charge) in the Department of Electrical and Electronic Engineering of Northern University of Business and Technology, Khulna, Khulna-9100, Bangladesh. He can be contacted at email: sohel.rana@uits.edu.bd.



Md. Abdur Razzak (Senior Member, IEEE)    received the B.Sc. degree (Hons.) in electrical and electronic engineering (EEE) from the Rajshahi University of Engineering and Technology (RUET), in 1995, and the M.Sc. and Ph.D. degrees in energy engineering from Nagoya University, Japan, in 2003 and 2006, respectively. He is currently a Professor of Electrical and Electronic Engineering (EEE) at Independent University, Bangladesh (IUB), where he has worked as the Head of the EEE Department, from 2016 to 2018. He has been invited more than 30 national and international conferences and universities as a keynote speaker. He also served as the expert member for graduate (M.Sc. and Ph.D.) examination committee in more than 25 universities at home and abroad. He has published more than 185 research articles in peer-reviewed journals and international conferences. His research interests include power electronics, renewable energy technologies, EV charging systems, and smart grid. He is a fellow of IEB. He received the Gold Medal from RUET for his B.Sc. degree. He was a recipient of the RUET Gold Medal, in 1995; the HKUST Fellowship, in 1999; the Japanese Government Scholarship, from 2000 to 2006; the IEEE Graduate Scholar Award, in 2005; the Hori Information Promotion Award, in 2005; the Japan Society for the Promotion of Science Postdoctoral Fellowship Award, in 2008; the Visiting Professorship at MJIT, University Technology Malaysia, in 2015; the IUB Teaching Excellence Award, in 2020; and the IUB Publication Excellence Award, in 2020. He has served as the general chair, the technical program chair, the technical program co-chair, the session chair, an international program committee member, an advisory board member, and an editorial board member for more than 50 journals and international conferences. He can be contacted at email: razzak@iub.edu.bd.